Korean J. Chem. Eng., 35(10), 2086-2096 (2018)
DOI: 10.1007/s11814-018-0124-7

pISSN: 0256-1115
eISSN: 1975-7220

Comparison study of naphthalene adsorption on activated carbons prepared from different raws

Pengyun Liu*, Zhansheng Wu*,†, Zhonghai Sun*, and Jun Ye**

*School of Chemistry and Chemical Engineering/The Key Lab. for Green Processing of Chemical Engineering of Xinjiang Bingtuan, Shihezi University, Shihezi 832003, P. R. China
**College of Materials Science and Engineering, State Key Laboratory of Organic-Inorganic Composites, Beijing University of Chemical Technology, Beijing 100029, P. R. China
(*Received 8 April 2018 • accepted 18 July 2018*)

Abstract−Five activated carbons (ACs) from apricot shells (ACAS), mixture of lignin and cellulose (ACLC), wood (ACW), walnut shells (ACWS), and coal (CAC) were prepared and used as adsorbents to study the adsorption behavior of naphthalene. All ACs were characterized by scanning electron microscopy, N_2 adsorption-desorption method, X-ray photoelectron spectroscopy, and elemental analysis. The effects of initial concentration, contact time, ionic strength, pH, and temperature on the adsorption of ACs for naphthalene were examined. Results show that CAC exhibit higher micropore specific surface area and contain more C-O bond than other ACs. Except for ACW, CAC is the least polar or the most hydrophobic adsorbent among ACs. This finding may be helpful in the formation of hydrogen bonding between CAC and naphthalene. The adsorption quantity of CAC was 227.03 mg g^{-1} at 303 K, which was considerably higher compared with that of other ACs. The kinetics process of naphthalene on all ACs was controlled by pseudo-second-order kinetic model. The adsorption equilibrium of naphthalene on ACs was reached at 40 min. The adsorption isotherms of naphthalene to ACs were consistent with the Freundlich isotherm model. The result of thermodynamic analysis shows that the adsorption occurs spontaneously. Moreover, the higher starting naphthalene concentration and lower adsorption temperature significantly can enhance the adsorption capacity of CAC. The maximum adsorption value of naphthalene on ACs was also observed at pH 4 under the same conditions. Moreover, the increase in ionic strength slightly promotes the adsorption of naphthalene on ACs. The microporous structure, element content and surface functional group of ACs affect its adsorption capacity.

Keywords: Activated Carbon, Adsorption, Naphthalene, Different Raws, Comparison

INTRODUCTION

Polycyclic aromatic hydrocarbons (PAHs), permanent organic pollutants composed of multiple aromatic rings (≥2); these compounds are mutagenic, carcinogenic and teratogenic [1]. PAHs cannot be easily biodegraded owing to their molecular structure stability and semi-volatile characteristic [2] and can be transported for long distances in environmental medium. Naphthalene, one of the significant PAHs containing two benzene rings, is a hydrophobic compound that can accumulate in soils or water for a long period. In the industrial field, naphthalene is a widespread precursor for the preparation of fuel, solvent, resin, and other materials [3] and can be easily exposed to the environment. In addition, naphthalene is belonging to the 16 PAHs as priority pollutants [4], and be widely investigated due to its excellent water solubility [5].

Compared with some methods reported for naphthalene removal, adsorption is superior to other wastewater decontamination techniques, thanks to its efficient adsorption capacity and simple operation [6]. Moreover, adsorbents from low-cost and easy-collect raws should be developed for removing PAHs from wastewater. Recently, activated carbon (AC) has been widely used for adsorption in terms of its superior specific surface area, microporous character and the surface chemical nature [7]. At present, numerous raw materials, such as coconut shell [8], camellia sinensis leaves [9], apricot shells [10], lignocellulosic [11], wood [12], walnut shells [13], and coal [2], can be used to prepare AC. Lignocellulosic materials, which contain cellulose, hemicellulose, and lignin components [14], have been utilized in AC preparation. These rich-cellulose materials contain a considerable amount of carbon, which contributes the high yield and heterogeneous porosity of the ACs.

The physical and chemical properties of ACs generally depend on treatment conditions and the selected raw materials. Structural differences between the ACs produced under identical conditions may be related to the composition of the precursors [15]. These properties and structure may be related to their effectiveness in AC applications and are important for commercial utilization [15]. The prepared ACs from apricot shell [10], wood sawdust [12], lignin, cellulose [11], walnut shell [13], and coal [2], are reportedly used for the adsorption of aromatic organics. As a typical natural waste, apricot shell mainly consists of cellulose, hemicellulose, and lignin [16], which may form carbon after pyrolysis at high temperature. Wood sawdust mostly contains holocellulose and a small part of the

†To whom correspondence should be addressed.
E-mail: wuzhans@126.com

lignin; moreover, wood sawdust is extractive, and its ash can be used to prepare AC as a sustainable development goal [17]. AC derived from walnut shell with high fixed carbon content and low ash content exhibits high surface area and pore volume [18]. Coal-based activated carbon (CAC) derived from anthracite offer several advantages, such as structural stability, high mechanical strength, good wear resistance, low adsorption energy, and easy regeneration [2]. However, to our knowledge, there are only few reports comparing the performance of these ACs in naphthalene removal.

Our study aim was to evaluate the difference in naphthalene adsorption on five kinds of ACs prepared from different raw materials, such as three commercial ACs, apricot shell AC (ACAS), wood AC (ACW), and walnut shell AC (ACWS), as well as two kinds of self-made ACs: lignin and cellulose-based AC (ACLC) and CAC. We also explored the intrinsic link between pore structure and surface properties of ACs, and their amount of adsorption. The adsorption kinetics, isotherm and thermodynamics of naphthalene on five kinds of ACs were explored to reveal the adsorption mechanisms. The influences of pH and ionic strength on ACs for naphthalene adsorption in aqueous solution were also investigated to determine the dominant adsorption properties.

MATERIALS AND METHODS

1. Materials

Three types of commercial ACs (ACAS, ACW, and ACWS) were brought from Henan Zhongbang Environmental Technology Co., Ltd., China. The naphthalene (≥97%) was purchased from Shanghai Tianlong Chemical Co., China. All chemical reagents and chemicals were of analytical grade.

2. Preparation of CAC and ACLC

The anthracite, purchased from TBEA Xinjiang, China, was crushed and sieved through 100 meshes for the preparation of CAC. Then the pulverized coal was washed with distilled water and dried in an air oven at 383 K for 4 h. CAC was prepared in a microwave reactor (MM823LA6-NS) by potassium hydroxide activation under vacuum atmosphere [2,3]. Lignin and cellulose (LC) were bought from Chengdu Kelon Chemical Reagent Field and Tianjin Guangfu Chemical Research Institute, China, respectively. LC was used to prepare ACLC by zinc chloride activation under microwave heating. The LC was mixed in a mass ratio of 1 : 1 to obtain a mixture LC, with a ratio of $ZnCl_2$/LC (w/w) of 1 : 1. Microwave power was 900 W, and radiation time was 15 min. The finished products were washed with 10% hydrochloric acid and then with distilled water until the pH level was approximately 7. The obtained AC samples were dried at 383 K for 4 h and designated as CAC and ACLC [3].

3. Characterization Methods

3-1. BET Surface Area and Pore Size Analysis

ACs surface area and pore size parameters were obtained from a Micromeritics ASAP 2020 surface area analyzer by N_2 adsorption-desorption method. The ACs were degassed under N_2 flow at 308 K for 6 h before adsorption isotherms were generated by N_2 at 77 K. The surface area (S_{BET}) was calculated with the Brunauer-Emmett-Teller (BET) equation, and the total pore volume (V_T, $m^3 g^{-1}$) was obtained from the adsorption isotherm at P/P_0=0.95. Micropore volume (V_{mic}) and area (S_{mic}) were estimated via t-plot method. The average pore size (r) was calculated by the Eq. (1):

$$r = \frac{4V_T}{S_{BET}} \quad (1)$$

3-2. XPS Analysis

The X-ray photoelectron spectroscopy (XPS) analysis involved using a PHI5700 ESCA system with a Mg Kα X-ray source (1,253.6 eV) under a vacuum pressure $<10^{-6}$ Pa. Wide scans were carried through in the range of 0 to 1,000 eV with a pass energy of 50 eV.

3-3. Elemental Analysis

Elemental analysis of carbon, hydrogen, nitrogen, sulfur, and oxygen of AC samples was performed using a Vario EL cube analyzer. Oxygen content was obtained by difference.

3-4. SEM Analysis

The textural structure of AC samples was characterized by scanning electron microscopy (SEM, JEOL, JSM-6490LV, Japan) with a secondary electron beam and an acceleration voltage of 30 kV. The samples were coated with gold to ensure suitable conductivity of particles after having been dried for 12 h at 353 K under vacuum.

4. Batch Adsorption Experiments

A series of adsorption studies were conducted by mixing 0.015 g of ACs with 100 mL of a certain concentrations naphthalene solution, and agitation at 120 r min^{-1} until the adsorption equilibrium of naphthalene was reached. The effects of the adsorption parameters such as initial naphthalene concentration (10-50 mg L^{-1}), contact time (0-80 min), temperature (288 K-318 K), pH (0-10), and ionic strength (0-1.0 mol L^{-1}) were systematically studied in the subsequent experiments. Determinations were conducted in duplicates.

5. Analysis

The adsorption capacities (mg g^{-1}) of five ACs were calculated according to the Eq. (2):

$$q_e = \frac{(C_0 - C_e)V}{m} \quad (2)$$

where C_0 and C_e (mg L^{-1}) are the naphthalene concentrations of before and after adsorption, respectively, m (g) is the mass of AC, V (L) is the volume of solution; q_e (mg g^{-1}) is the amount adsorbed per gram AC; and C_e (mg L^{-1}) is the equilibrium concentration of

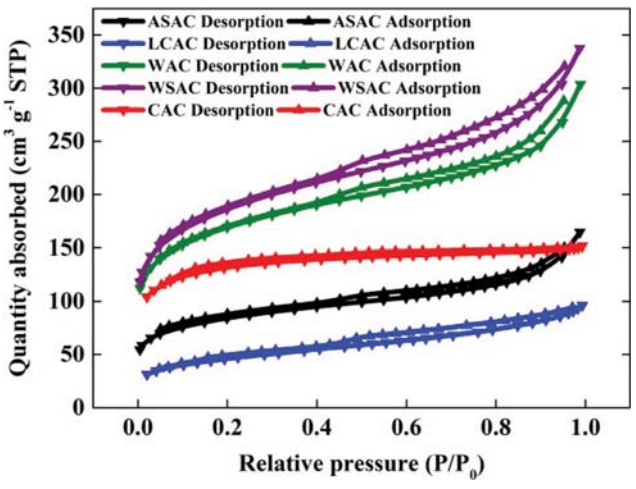

Fig. 1. The N_2 adsorption and desorption isotherms at 77 K of ACs.

Table 1. The BET analysis for ACs

Parameters	ACAS	ACLC	ACW	ACWS	CAC
BET specific surface area ($m^2 g^{-1}$)	276.2	154.2	553.3	614.2	401.7
Micropore specific surface area ($m^2 g^{-1}$)	84.6	93.5	160.5	166.7	337.3
External specific surface area ($m^2 g^{-1}$)	191.6	60.4	392.8	447.5	64.4
Total pore volume ($m^3 g^{-1}$)	0.21	0.13	0.41	0.46	0.21
Micropore volume ($m^3 g^{-1}$)	0.16	0.05	0.20	0.22	0.16
Average pore size (nm)	3.69	3.56	3.41	3.40	2.34

naphthalene solution.

RESULTS AND DISCUSSION

1. Characterizations of the ACs

1-1. N_2 adsorption-desorption isotherms

The N_2 adsorption-desorption isotherms of ACs were obtained (Fig. 1) to investigate the difference in surface textural properties of the five ACs. The N_2 adsorption isotherms of the ACs were of type I with a type-H_4 hysteresis loop according to IUPAC classification [2,7,18]. The equilibrium adsorption capacity of N_2 was as follows: ACWS>ACW>CAC>ACAS>ACLC. The N_2 adsorption rate of ACLC is lower than those of other ACs in the P/P_0 range, demonstrating that ACLC shows less porosity than other samples in the micro- and mesopore ranges [19]. According to pore size analysis (Table 1), the pore size of the five samples is located in the mesopore range, suggesting all of them are mesoporous materials. The pore size order is ACAS>ACLC>ACW>ACWS>CAC; the main reason is that the pore size of AC was closely related to its raw materials and activation process [15]. ACWS presented an extremely high surface area (614.2 $m^2 g^{-1}$), whereas CAC showed a high micropore specific surface area (337.3 $m^2 g^{-1}$). The microporosity is a desired characteristic of CAC to be versatile in application [20]. The microporous property of AC can provide abundant active sites that are helpful to the adsorption of naphthalene.

1-2. XPS Analysis

XPS is useful for analyzing the surface chemical composition of ACs by measuring the binding energy of electrons associated with atoms (Fig. 2). The two main peaks were identified and labeled as C 1*s* and O 1*s* of ACs. The order of C content was ACWS>ACW>ACAS>ACLC>CAC, and the order of O content was ACAS>ACW>CAC>ACWS>ACLC. The high-resolution spectra of O 1*s* were further analyzed by a curve-fitting procedure. Information concerning the components, and the assignments and peak parameters of different O 1*s* components of ACs are listed in Table 2.

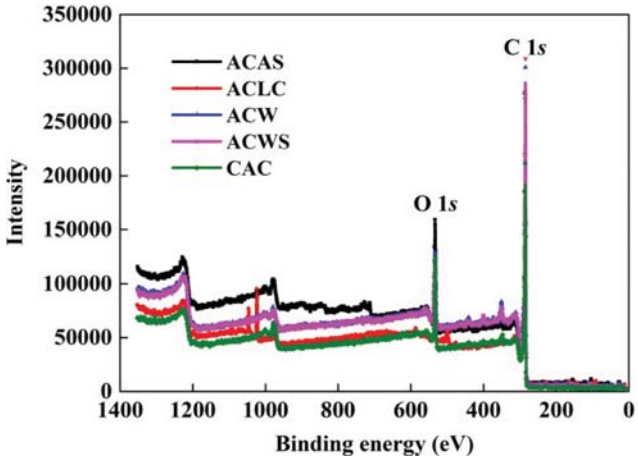

Fig. 2. The XPS survey scans of ACs.

Four peaks were derived from O 1*s* at 531.2, 532.4, 533.3, and 534.3 eV represented the groups of C=O, O-C, R-O*-C=O, and C-OOH, respectively [2,21]. For oxygen species, the content of oxygen-enriched groups of ACs from different raw materials varied. These results suggest that compared with the other ACs, ACLC and ACW contain more C=O and C-OOH groups, respectively, which may from π-π interaction as face-to-face stacking between the π-π* of ACs and the molecular of naphthalene. The C-O group was predominant in CAC because of its composition of 52.37% of the carbon species, which may form strong hydrogen bonds with H-rich naphthalene rings [22]. All of these findings can improve the AC adsorption capacity of naphthalene.

1-3. Elemental Contents Analysis

The elemental content analysis results show the five ACs possess similar elemental compositions (Table 3). Meanwhile, the reduction of O/C ratio in AC can be attributed to certain oxygen-enriched groups that were removed from the carbon surface [23].

Table 2. Assignments and peak parameters of different O 1*s* components of ACs

Components	Assignments	Binding energy (eV)	Concentration of each sample (%)				
			ACAS	ACLC	ACW	ACWS	CAC
O(1)	C=O	531.2	28.93	9.03	1.87	10.86	21.39
O(2)	C-O	532.4	31.62	47.51	16.78	16.52	52.37
O(3)	R-O*-C=O	533.3	18.48	32.05	0.94	25.60	17.53
O(4)	O*=C-OH	534.3	20.97	11.40	80.41	47.02	8.71

Table 3. The elemental analysis of ACs

ACs	N%	C%	H%	S%	O, diff%	N/C	H/C	O/C	(O+N+S)/C
ACAS	0.31	47.98	0.58	0.66	50.47	0.006	0.012	1.052	1.072
ACLC	0.54	54.95	3.10	5.49	35.92	0.010	0.056	0.654	0.764
ACW	0.30	72.86	0.52	1.32	25.00	0.004	0.007	0.341	0.363
ACWS	0.58	67.88	0.89	0.91	29.74	0.009	0.013	0.438	0.460
CAC	0.21	67.10	3.81	0.23	28.65	0.003	0.057	0.427	0.433

The ratios of H/C and O/C or O+C+N/C can be used to analyze the level of polarity and aromaticity of ACs [24]. The values of H/C ratio (0.012-0.067) suggested that the unsaturation in the carbon chains of ACs was high (H/C<0.5 is considered as high unsaturation), indicating the dominance of aromatic structures in the ACs [25]. The polarity of ACs varied in a certain range, and the CAC was the least polar adsorbent, except for ACW. In addition, the (O+N+S)/C ratio analysis showed that ACAS presented the highest (O+N+S)/C ratio (1.072), followed by ACLC (0.764), ACWS (0.460), CAC (0.433), and ACW (0.363). The (O+N+S)/C also exhibited a decrease, indicating that the polarity of ACs weakened in turn, which possibly contributed to the increased affinity of naphthalene on ACs for adsorption [24]. These results were also confirmed by the XPS analysis results.

1-4. SEM Analysis

Fig. 3 shows SEM photographs of the five ACs, which exhibit different surface characteristics in Fig. 3. SEM images of ACs provide critical information on pore texture and surface heterogeneity. The outer surface structure is extremely rough, presenting small cavities on the surface; this finding indicates the presence of an interconnected porous structure in ACs as a result of pyrolysis process [2,26]. This observation shows that the external surfaces of ACAS, ACLC, ACW, and ACWS displayed an extremely disorder pore structure. By contrast, the CAC clearly had relatively good pore structure, which confers good adsorption capacity for naphthalene in waste water.

2. Adsorption Kinetics of Naphthalene on ACs

The adsorption kinetics process can be analyzed by pseudo-first-order (Eq. (3)), pseudo-second-order (Eq. (4)) kinetic models, and Elovich equation (Eq. (5)).

2-1. Pseudo-first-order Kinetic Model

The pseudo-first-order kinetic model of naphthalene adsorption on ACs [3] is expressed as:

$$\ln(q_e - q_t) = \ln q_e - \frac{K_1}{2.303}t \quad (3)$$

where q_e and q_t (mg g^{-1}) correspond to the adsorbed amounts at the equilibrium and time t (min), respectively. The K_1 (min^{-1}) represents the adsorption rate constant of pseudo-first-order, which was yielded from the linear plot of ln (q_e–q_t) against t [2]. The model parameters of K_1, q_e and R^2 (correlation coefficients) are presented in Table 4; there was an obviously value-gap between values of q_e experimental ($q_{e,exp}$) and q_e calculated ($q_{e,cal}$).

2-2. Pseudo-second-order Kinetic Model

The pseudo-second-order kinetic rate equation of naphthalene adsorption on ACs is expressed [27] by:

$$\frac{t}{q_t} = \frac{1}{K_2 q_e^2} + \frac{t}{q_e} \quad (4)$$

where K_2 (g mg^{-1} min^{-1}) is the adsorption rate constant of pseudo-second-order [28]. The plot of t/q_t versus t was used to evaluate experimental data, and the linear slope and intercept were related

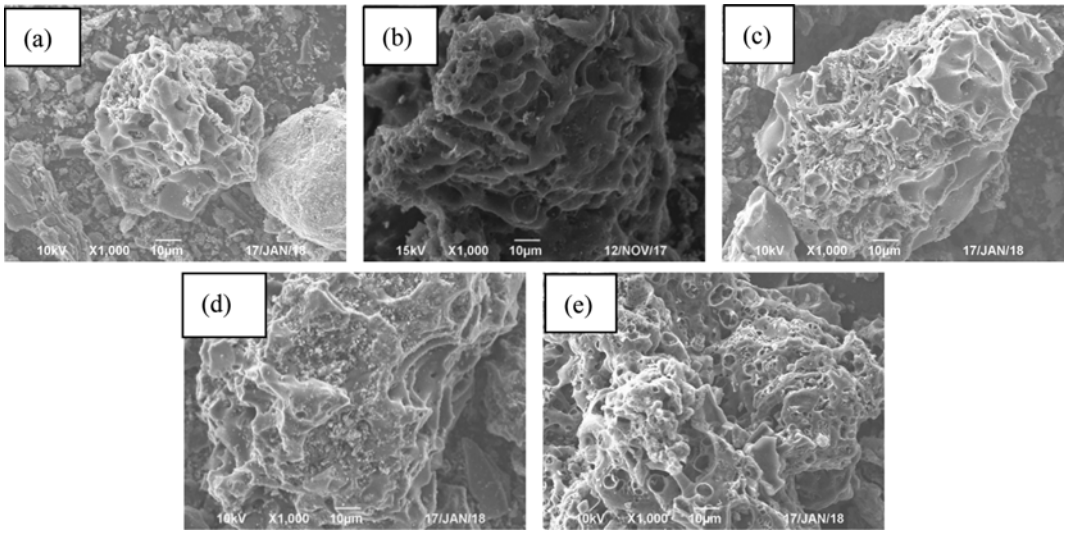

Fig. 3. The SEM images of ACs. (a) ACAS, (b) ACLC, (c) ACW, (d) ACWS, (e) CAC.

Table 4. Adsorption kinetic parameters of naphthalene onto ACs at 303 K

ACs	C_0 (mg L^{-1})	q_{exp} (mg g^{-1})	Pseudo-first-order			Pseudo-second-order			Elovich equation			
			$q_{e,cal}$ (mg g^{-1})	K_1 (min^{-1})	R^2	$q_{e,cal}$ (mg g^{-1})	K_2 (g mg^{-1} min^{-1})	R^2	$q_{e,cal}$ (mg g^{-1})	$(1/\beta)\ln(\alpha\beta)$ (mg g^{-1})	$1/\beta$	R^2
ACAS	10	51.18	18.23	0.066	0.8562	53.36	0.01425	0.9996	55.59	26.15	6.72	0.9392
	20	60.63	50.51	0.075	0.9511	62.50	0.00692	0.9992	65.40	23.83	9.49	0.9638
	30	83.56	11.19	0.043	0.6295	84.03	0.02321	0.9999	86.72	64.54	5.06	0.9359
	40	104.30	30.58	0.058	0.6787	106.38	0.00593	0.9991	110.46	54.06	12.87	0.8992
	50	152.01	39.43	0.069	0.8450	153.85	0.00571	0.9991	153.11	104.25	11.15	0.8162
ACLC	10	52.85	23.59	0.049	0.8069	54.95	0.00700	0.9992	57.25	18.77	8.78	0.9634
	20	89.91	14.09	0.043	0.7255	93.46	0.01817	0.9999	95.44	71.68	5.42	0.9600
	30	95.87	25.74	0.049	0.8444	97.09	0.00870	0.9992	97.34	64.19	7.57	0.9750
	40	149.86	59.40	0.061	0.8460	153.85	0.00343	0.9991	156.40	74.30	18.74	0.9698
	50	153.33	46.08	0.057	0.8499	156.25	0.00465	0.9991	154.49	99.32	12.59	0.9414
ACW	10	54.82	10.95	0.068	0.8814	55.25	0.02776	0.9998	56.92	39.75	3.92	0.8543
	20	95.88	41.45	0.067	0.9408	98.04	0.00608	0.9991	99.64	51.46	10.99	0.9815
	30	123.14	52.38	0.059	0.8486	125.00	0.00496	0.9991	127.22	68.27	13.45	0.9523
	40	176.47	24.41	0.060	0.9305	178.57	0.01161	0.9998	177.38	148.56	6.58	0.9191
	50	182.94	54.59	0.059	0.8429	185.19	0.00429	0.9991	182.16	126.80	12.63	0.8792
ACWS	10	55.95	12.75	0.068	0.9551	56.50	0.02506	0.9998	57.56	41.16	3.74	0.9404
	20	103.22	42.12	0.081	0.9869	105.26	0.00679	0.9991	105.86	63.35	9.67	0.9458
	30	162.02	14.80	0.055	0.4835	158.73	0.02335	1.0000	160.78	139.97	4.75	0.9555
	40	188.78	67.64	0.072	0.9117	178.57	0.00490	0.9992	186.48	126.48	13.69	0.9200
	50	194.58	40.32	0.060	0.7251	196.08	0.00565	0.9996	196.64	143.32	12.17	0.9703
CAC	10	56.76	13.70	0.051	0.5362	57.47	0.01346	0.9992	57.13	37.61	4.45	0.9369
	20	113.79	26.18	0.196	0.8455	114.94	0.01428	0.9998	116.70	85.68	7.10	0.8637
	30	160.72	14.26	0.041	0.8004	161.29	0.01922	0.9999	163.18	140.43	5.19	0.9729
	40	191.44	74.61	0.058	0.9739	200.00	0.00287	0.9992	194.56	108.47	19.65	0.9659
	50	219.52	80.24	0.066	0.8491	222.22	0.00277	0.9991	227.03	121.27	24.14	0.9797

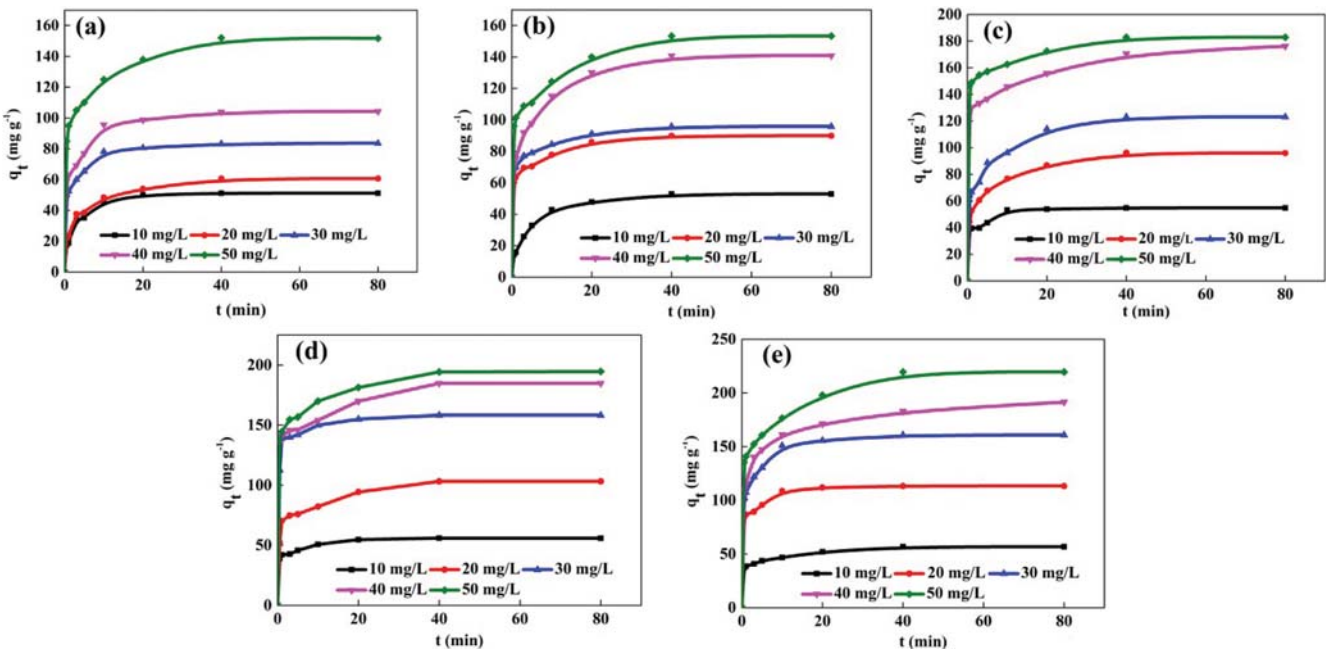

Fig. 4. The effect of time on the adsorption quantity of ACs at 303 K. (a) ACAS, (b) ACLC, (c) ACW, (d) ACWS, (e) CAC.

to values of q_e and K_2 in Table 4. The R^2 values always exceed 0.99 when initial naphthalene concentration ranges from 10-50 mg L^{-1}, suggesting that the current model describes the adsorption process well and the $q_{e,cal}$ values extremely close to the $q_{e,exp}$ values. A similar situation was founded in the removal of naphthalene by CAC [7]. The curves of adsorption capacity with contact time are shown in Fig. 4. The adsorption curves of naphthalene on ACs exhibited a similar trend. At the stage of 0-10 min, adsorption occurred rapidly. With the extension of adsorption time, the amount of adsorbed naphthalene gradually reaches the maximum value at 40 min, similar adsorption processes have been reported in the literature [2]. The graph also revealed that CAC exhibits higher naphthalene adsorption capacity than ACAS, ACLC, ACW, and ACWS. This order is consistent with the microporous structure analysis in Table 1. Thus, we concluded that the existing mesopores and great pore properties of CAC can be propitious to naphthalene adsorption. Moreover, a significant discrepancy exists in the adsorption of naphthalene with different concentrations on ACs. The CAC adsorption capacity can achieve 2.87-fold adsorption when the naphthalene concentrations increase from 10 to 50 mg L^{-1}. This outcome may be due to the increased concentration of naphthalene, which enhances the concentration difference between the aqueous solution and the liquid film of AC external surface, thereby enhancing the transfer of naphthalene into the pores of the AC [2]. The maximum adsorption value of CAC was 227.03 mg g^{-1} at naphthalene concentration of 50 mg g^{-1} at 303 K.

2-3. Elovich Equation

The relationship is usually applied when the adopted adsorbent surface is heterogeneous [29]. The Elovich equation of naphthalene adsorption on ACs is given as Eq. (5):

$$q_t = \frac{1}{\beta}\ln(\alpha\beta) + \frac{1}{\beta}\ln(t) \tag{5}$$

where α (mg g^{-1} min^{-1}) is the starting adsorption rate, and β (g mg^{-1}) is used to evaluate the activation energy (E_a) for chemisorption and the degree of surface coverage. The value of ($1/\beta$) corresponds to the slope of the linear plot of q_t versus ln(t), whereas while the ($1/\beta$)ln($\alpha\beta$) corresponds to the intercept, both of them are helpful in understanding the adsorption behavior of the first step [30]. The R^2 values in Elovich equation ranged from 0.82-0.98 for the starting naphthalene concentration of 10-50 mg L^{-1}, and the $q_{e,cal}$ values obtained from Eq. (5) fitted well with the $q_{e,exp}$ values to a certain extent (Table 4).

3. Adsorption Isotherms of Naphthalene on ACs

Adsorption isotherms are usually in favor of implementing realistic applications and can be used to determine the adsorption mechanism. Four isotherm models, Langmuir, Freundlich, Temkin, and Dubinin-Radushkevich, were investigated to evaluate the adsorption behavior and applied to experimental data. Origin Pro 9.0 was used for these calculations.

3-1. Langmuir Isotherm Model

The Langmuir isotherm model is applied to the adsorption system contains a homogeneous ACs surface, which is written as [2]:

$$\frac{C_e}{q_e} = \frac{1}{q_m}C_e + \frac{1}{q_m K_L} \tag{6}$$

where C_e (mg L^{-1}) is the adsorbate concentration in the solution, q_m (mg g^{-1}) is the maximal adsorption amount of naphthalene, and K_L (L mg^{-1}) is a constant corresponding to the adsorption free energy (E).

3-2. Freundlich Isotherm Model

The Freundlich isotherm model of naphthalene adsorption on ACs is an empirical equation, this model can be expressed as [3]:

$$q_e = K_F C_e^{1/n} \tag{7}$$

where K_F (L mg^{-1}) is o the constant of adsorption capacity and n is the constant of adsorption intensity.

3-3. Temkin Isotherm Model

The Temkin isotherm model of naphthalene adsorption on ACs is expressed as [30]:

$$q_e = \left(\frac{RT}{b_T}\right)\ln(AC_e) \tag{8}$$

$$B = \frac{RT}{b_T} \tag{9}$$

$$q_e = B\ln A + B\ln C_e \tag{10}$$

where B (J mol^{-1}) is the constant representing sorption heat, and A (L mg^{-1}) is the equilibrium binding parameter. R (8.314 J mol^{-1} K^{-1}) and T (K) are the universal gas constant and absolute temperature of solution, respectively.

3-4. Dubinin-Radushkevich Isotherm Model

Dubinin-Radushkevich isotherm model of naphthalene adsorption on ACs is defined as [30]:

$$q_e = q_s \exp(-B_{DR}\varepsilon^2) \tag{11}$$

$$\ln q_e = \ln q_s - B_{DR}\varepsilon^2 \tag{12}$$

where ε can be correlated as:

$$\varepsilon = RT\ln\left(1+\frac{1}{C_e}\right) \tag{13}$$

where constant B_{DR} endues the mean E of naphthalene sorption during transfer to the ACs surface from the solution. The constant can be calculated by Eq. (14) [24]:

$$E = \left[\frac{1}{\sqrt{2B_{DR}}}\right] \tag{14}$$

Parameters of E and q_s can be determined from the plot of ln q_e versus ε^2.

Fig. 5 presents the plot of q_e versus C_e of naphthalene adsorption on ACs at different temperature, and the curves of all the five samples exhibit similar trends. The values of q_m, K_L, K_F, and n were determined by nonlinear regression analysis (Table 5). I.A. Tan believes the sorption process is favorable when 1/n values lie between 0.1 and 1 [31], and all 1/n values obtained are in this range according to our analysis results, indicating that the current naphthalene adsorption on ACs is favorable. In addition, the R^2 exceeds 0.99 for Freundlich models, suggesting that the Freundlich isotherm is a better description of the sorption equilibrium data. The parameter R^2 values of Temkin and Dubinin-Radushkevich isotherm models are lower than those of other isotherm models,

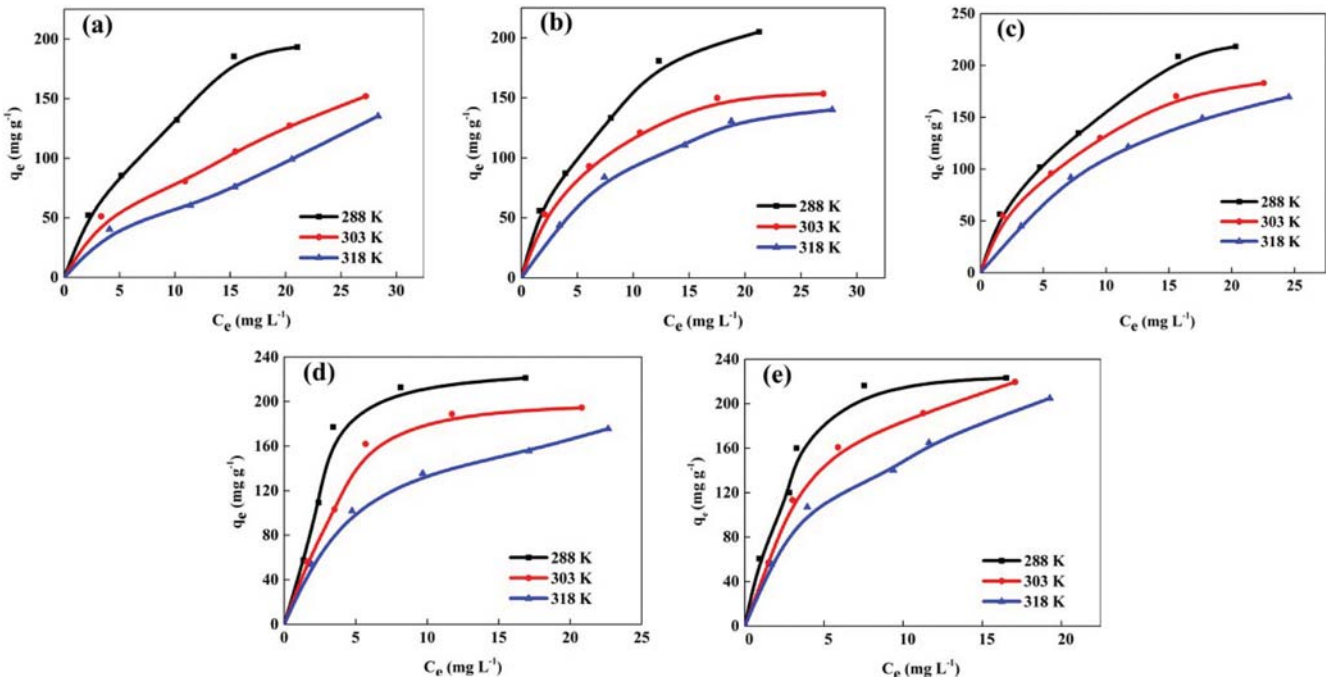

Fig. 5. Experimental naphthalene adsorption isotherms on ACs ((a) ACAS, (b) ACLC, (c) ACW, (d) ACWS, (e) CAC) at pH 7 and at 288 K, 303 K, and 318 K.

Table 5. Langmuir, Freundlich, Temkin, and Dubinin-Radushkevich isotherm model constants and correlation coefficients (303 K)

Isotherm model	Parameters	ACs				
		ACAS	ACLC	ACW	ACWS	CAC
Langmuir	q_{max} (mg g^{-1})	175.44	178.57	243.90	243.90	322.58
	K_L (L mg^{-1})	0.0754	0.1564	0.1302	0.2113	0.1640
	R^2	0.6297	0.8544	0.9197	0.9662	0.9571
Freundlich	K_F (L mg^{-1})	17.79	39.17	41.08	43.66	58.96
	1/n	0.7145	0.4267	0.4846	0.5646	0.4819
	R^2	0.9902	0.9914	0.9846	0.9902	0.9934
Temkin	A (L mg^{-1})	1.4406	1.8877	1.3833	1.7855	1.7587
	B	31.31	37.28	52.34	58.09	65.32
	R^2	0.6037	0.8132	0.8983	0.8954	0.9915
Dubinin-Radushkevich	q_s (mg g^{-1})	96.96	126.01	148.83	175.25	193.91
	E (J mol^{-1})	0.7895	0.7534	0.7899	0.7999	0.8244
	R^2	0.4438	0.7749	0.7973	0.8775	0.9601

demonstrating that these two models failed to describe the naphthalene adsorption process in this study.

With the increase in temperature, the values of K_L, K_F, and n decreased (Table 5). This finding reveals that temperature negatively affects the adsorption of naphthalene onto ACs possibly because the naphthalene adsorption is exothermic [2].

4. Adsorption Thermodynamics and Activation Energy

The E_a of naphthalene adsorption on ACs is obtained from Arrhenius Eq. (15) [24]:

$$\ln K_2 = \ln A - \frac{E_a}{RT} \quad (15)$$

The value of free-energy change (ΔG, kJ mol^{-1}) was determined by Eq. (16), and the values of enthalpy change (ΔH, kJ mol^{-1}) and entropy change (ΔS, J K^{-1} mol^{-1}) were identified by Eq. (18), which was derived by Eq. (16) and Eq. (17). According to Eq. (18), the plot of lnK_F versus 1/T was obtained and the slope and intercept of which can be used to calculate the ΔH and the ΔS, respectively [31]. The thermodynamic equations of naphthalene adsorption on ACs were written as follows [2]:

$$\Delta G = -RT\ln K_F \quad (16)$$

$$\Delta G = \Delta H - T\Delta S \quad (17)$$

$$\ln K_F = \frac{\Delta S}{R} - \frac{\Delta H}{RT} \quad (18)$$

Table 6. Thermodynamic parameters for the adsorption of naphthalene in aqueous solution onto ACs

ACs	ΔH (KJ mol^{-1})	ΔS (J mol^{-1} k^{-1})	E_a (KJ mol^{-1})	ΔG (KJ mol^{-1})		
				288 K	303 K	318 K
ACAS	−26.87	63.18	35.12	−6.18	−7.73	−8.37
ACLC	−14.90	19.32	31.71	−8.42	−9.05	−9.39
ACW	−15.45	20.51	25.33	−8.61	−9.26	−9.51
ACWS	−9.52	1.40	5.68	−9.67	−10.06	−10.13
CAC	−13.18	8.99	1.36	−10.25	−10.44	−10.53

The highest and lowest adsorption capacities were observed at 288 K and 318 K, respectively (Table 6). Low values of E_a are a property for physisorption, indicating that the physical adsorption is the leading adsorption process of naphthalene.

The negative ΔG values revealed that the process of naphthalene adsorption on ACs was spontaneous. The ΔH<0 indicates the adsorption process is an exothermal. The ΔS>0 shows naphthalene adsorption onto ACs is entropically driven [3,31]. In summary, the thermodynamics research demonstrates that the adsorption of naphthalene onto ACs is a complex process.

The values q_e of naphthalene on various adsorbents were compared, and the results indicated that the CAC obtained by microwave assisted potassium hydroxide activation from coal powder is a potential adsorbent for the removal of naphthalene from water (Table 7).

5. Adsorption Mechanisms

The adsorption mechanisms of naphthalene may occur on the AC surface at the initial step, intraparticle diffusion, and diffusion through the boundary layer. In addition, intraparticle diffusion model of naphthalene adsorption on ACs can be expressed by the equation [24]:

$$q_t = K_p t^{1/2} + C \quad (19)$$

where K_p (mg g^{-1} min$^{-1/2}$) is the intraparticle diffusion constant, and C the thickness of the boundary layer. K_p and R^2 are calculated the plot of q_t versus $t^{1/2}$ [24].

The Boyd kinetic equation [31] was adopted to explain film-diffusion and intraparticle diffusion and determine the rate-limiting step in naphthalene adsorption. The Boyd equation is [24]:

$$-\ln\left(1-\frac{q_t}{q_e}\right) = K_{bf} t \quad (20)$$

where K_{bf} is liquid-film diffusion. A plot of ln (q_t/q_e−1) versus t is used to fit Boyd kinetic equations, and K_{bf} is obtained from the slope.

Fig. 6(a) shows the Weber-Morris plots. The adsorption fold line of naphthalene on ACs at the beginning stage is a precipitous

Table 7. Comparison of equilibrium adsorption capacity of naphthalene on various adsorbents

Adsorbents	Initial concentration (mg L^{-1})	Temperature (K)	Adsorption capcity (mg g^{-1})	References
Modified zeolite	1	303	0.3	[1]
Modified coal-based AC	30	298	131.2	[2]
Modified walnut shells	25	298	7.2	[32]
ZnS-NPs-AC	50	298	142.7	[33]
Modified hazelnut shell	25	298	17.3	[39]
ACLC	30	303	95.9	This work
CAC	30	303	160.7	This work

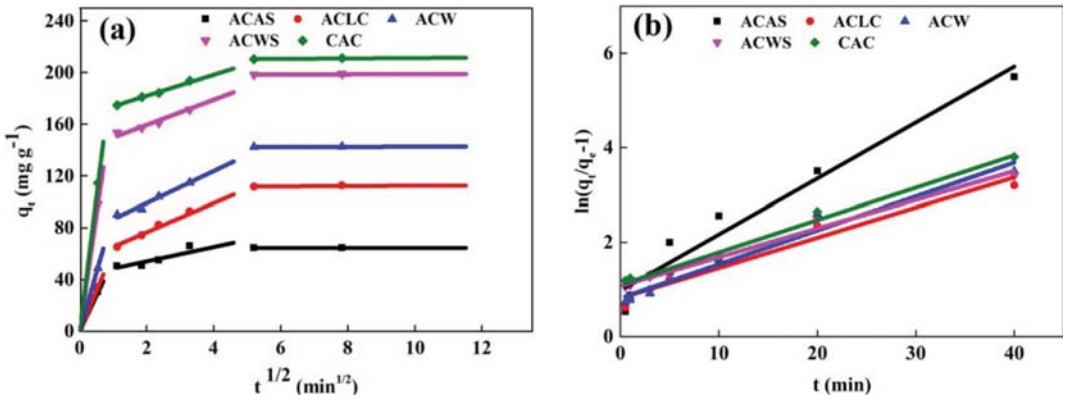

Fig. 6. Plot of intraparticle diffusion and film diffusion model for the adsorption of naphthalene onto ACs at 303 K.

Table 8. Intraparticle diffusion and film diffusion parameters of ACs at 303 K

ACs	Intraparticle diffusion model						Film diffusion model	
	K_{p1} (mg g^{-1} $h^{-1/2}$)	K_{p2} (mg g^{-1} $h^{-1/2}$)	K_{p3} (mg g^{-1} $h^{-1/2}$)	$(R_1)^2$	$(R_2)^2$	$(R_3)^2$	K_{bf} (min^{-1})	R^2
ACAS	54.95	4.89	0.95	0.99	0.86	0.99	0.12	0.95
ACLC	62.69	9.88	0.98	0.99	0.98	0.99	0.06	0.96
ACW	90.89	10.88	0.98	0.98	0.98	0.99	0.07	0.96
ACWS	179.69	8.56	0.99	0.98	0.99	0.99	0.06	0.98
CAC	207.24	7.17	0.99	0.99	0.99	0.99	0.07	0.98

line. The line then becomes gradually gentle until no significant changes are observed. This outcome suggests that the three-stage lines gradually changed from steep to gentle and the adsorption rate decreased slowly. The phenomenon may be attributed to the increase in film diffusion resistance when the naphthalene molecules diffused into the microporous structure and then were adsorbed on the inner surface of the AC; thus the diffusion rate decreased [34]. In addition, Fig. 6(a) shows the second- and third-stages line for each AC sample that did not pass through the origin, illustrating that intraparticle diffusion was not the only rate-controlled step [31]. The values of K_{p1}, K_{p2}, K_{p3}, and R^2 are shown in Table 8. The order of first-stage line slope (K_{p1}) of ACs is CAC> ACWS>ACW>ACLC>ACAS, which is consistent with the order of maximum adsorption of naphthalene on ACs under the same condition. Meanwhile, the second stage line slope (K_{p2}) of ACAS is lower than that of four other samples. Therefore, this finding may serve as evidence of the low adsorption capacity of ACAS. We believe that the other mechanisms possibly exist in adsorption.

The following analysis was conducted to clarify the adsorption mechanism of naphthalene onto ACs. The specific surface area, microstructure, pore size, and polarity of the ACs also play key roles during naphthalene adsorption process [35]. The adsorption capacity of naphthalene on CAC is higher than those of ACAS, ACLC, ACW, and ACWS. This higher capacity may be due to the higher micropore amount of CAC and higher π-π interactions between the aromatic rings on CAC and the heterocyclic ring of naphthalene in comparison with the other four ACs. Moreover, the dispersion forces between the π electrons of the other four adsorbents and naphthalene weakened because of more oxygen functional groups in the four ACs than those in CAC [36].

With the aim to obtain the practical rate-limiting step existing during adsorption, we show the Boyd's plot for the adsorption of naphthalene onto ACs in Fig. 6(b). The straight lines for all ACs did not pass through the origin and the points were scattered. These plots suggest that the adsorption of naphthalene on five ACs is dominant followed by external mass transport where particle diffusion is the rate-limiting step [30]. Table 8 presents the K_{bf} and R^2 of the Boyd's model for different ACs. Similar discovery was reported that the adsorption processes of cadmium ion on surface-modified AC were governed mainly by external mass transport [31].

6. Effect of Initial pH

The adsorption of naphthalene on ACs at different pH was performed by increasing pH from 2 to 10; the results are shown in Fig. 7. A substantial difference in the adsorption capacity of ACs was observed in the experiment. The maximum adsorption capacity occurred in pH 4. The adsorption capacity of naphthalene on ACAS, ACLC, ACW, ACWS, and CAC at pH 4 and 303 K was 93.37, 110.50, 148.24, 154.57, and 162.38 mg g^{-1}, respectively. Similar phenomenon happened in the removal of naphthalene by talc and graphene [37]. At low pH, abundant H^+ is easily adhered on the ACs surface, significantly increasing the hydrophilicity properties of the ACs. Abundant negative charges existed on ACs surface at high pH. Thus, electrostatic interaction between the ACs and naphthalene was enhanced, thereby overcoming the binding force. The combined effects may be attributed to the slight reduction in the adsorption capacity of adsorbents at high pH [9].

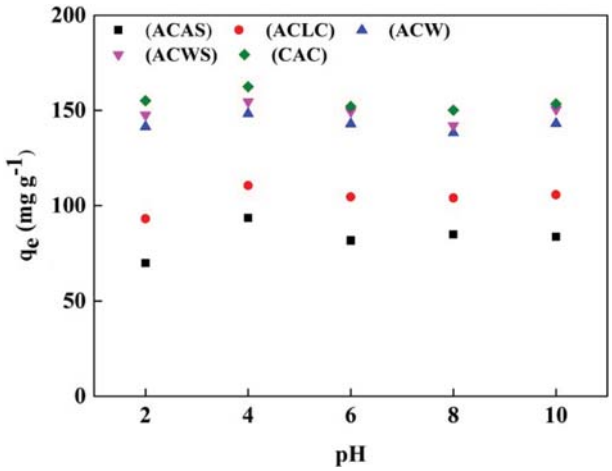

Fig. 7. Influence of pH of solution on the adsorption of naphthalene on ACs (Conditions: initial naphthalene concentration 30 mg L^{-1}, sorbent dosage 0.015 g, temperature 303 K, contect time 40 min).

7. Effect of Ionic Strength

The adsorption of naphthalene on ACs at different NaCl contents was performed (Fig. 8). The removal rate increments of naphthalene on ACAS, ACLC, ACW, ACWS, and CAC were 21.0%, 16.7%, 17.9%, 7.7%, and 2.2% when the concentration of Na^+ varied from 0.1 to 1.0 mol L^{-1}, respectively. These results demonstrated that the naphthalene removal efficiency exerts low responsiveness towards ionic strength and the naphthalene removal rates were promoted limitedly by increasing the content of Na^+ in the adsorption system. Similar result was also observed in the removal of bisphenol by a natural biosorbent and modified peat [38]. In addition, the promotion of the removal rate on CAC and ACWS was lower than that of other three ACs, indicating that different responsiveness between the concentration of Na^+ and ACs.

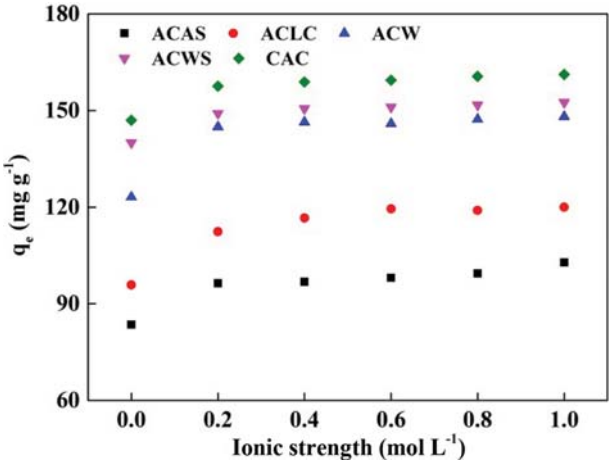

Fig. 8. Effect of ionic strength on naphthalene adsorption capacity on ACs (Conditions: naphthalene concentration 30 mg L^{-1}, sorbent dosage 0.015 g, pH 7, temperature 303 K contact time 40 min).

The slight promotion in the adsorption amount of naphthalene was caused by the following reasons. First, Na^+ combined with the opposite charge group from the surface of the ACs, which weakened the electrostatic interaction between naphthalene and ACs. Second, the content of electrolyte in solution was increased when the concentration of NaCl varied from 0.1 to 1.0, which would build stronger interaction with water molecules than that of naphthalene molecules, resulting in enhancing the adsorption of naphthalene on the surface of ACs [39].

CONCLUSIONS

The present study shows that the microporous structure, porosity, pore structure, π-π, and H-bond content of ACs would affect its adsorption capacity to naphthalene. The CAC has the highest micropore specific surface area and lower polar. In addition, CAC contains more C-O bond and has more complete pores than ACAS, ACLC, ACW, and ACWS, which may be helpful to adsorb large amounts of naphthalene. The order of naphthalene-adsorbed capacity is CAC>ACWS>ACW>ACLC>ACAS, and the adsorption quantity of CAC was 227.03 mg g^{-1} at 303 K. The adsorption kinetics of naphthalene on all ACs was controlled by the pseudo-second-order model. The adsorption equilibrium of naphthalene on ACs was reached at 40 min. The adsorption isotherms of naphthalene to ACs fit the Freundlich isotherm model. Increasing the initial concentration of naphthalene (0-50 mg L^{-1}) significantly enhances the adsorption capacity of CAC (73.9%). The adsorption of naphthalene on ACs is divided into three stages, and mass transport of particle diffusion is the rate limiting step. The largest amount of adsorbed naphthalene on ACs was observed consistently at pH 4 with the other conditions. Moreover, the increase in ionic strength slightly promotes the adsorption of naphthalene on ACs.

ACKNOWLEDGEMENTS

This work was supported financially by funding from the International Science and Technology Cooperation Program of Shihezi University (GJHZ201601) and the National Natural Science Foundation of China (21868034).

REFERENCES

1. N. Li, W. Cheng and Y. Pan, *J. Environ. Prot. Ecol.*, **8**, 416 (2017).
2. X. Ge, F. Tian, Z. Wu, Y. Yan, G. Cravotto and Z. Wu, *Chem. Eng. Process.*, **91**, 67 (2015).
3. Z. Sun, Z. Wu, D. Liu and X. He, *Korean J. Chem. Eng.*, **35**, 557 (2018).
4. S. S. Cai, J. A. Syage, K. A. Hanold and M. P. Balogh, *Anal. Chem.*, **81**, 2123 (2009).
5. B. Cabal, T. Budinova, C. O. Ania, B. Tsyntsarski, J. B. Parra and B. Petrova, *J. Hazard. Mater.*, **161**, 1150 (2009).
6. S. Gan, E. V. Lau and H. K. Ng, *J. Hazard. Mater.*, **172**, 532 (2009).
7. A. Regti, M. R. Laamari, S. E. Stiriba and M. E. Haddad, *Microchem. J.*, **130**, 129 (2017).
8. A. M. Aljeboree, A. N. Alshirifi and A. F. Alkaim, *Arab. J. Chem.*, **150**, S3381 (2014).
9. T. Mahmood, R. Ali, A. Naeem, M. Hamayun and M. Aslam, *Process Saf. Environ. Prot.*, **109**, 548 (2017).
10. M. H. Marzbali, M. Esmaieli, H. Abolghasemi and M. H. Marzbali, *Process Saf. Environ. Prot.*, **102**, 700 (2016).
11. S. I. Mussatto, M. Fernandes, G. J. M. Rocha, J. J. M. Órfão, J. A. Teixeira and I. C. Roberto, *Bioresour. Technol.*, **101**, 2450 (2010).
12. K. Y. Foo and B. H. Hameed, *Bioresour. Technol.*, **111**, 425 (2012).
13. G. Nazari, H. Abolghasemi, M. Esmaieli and E. Sadeghi Pouya, *Appl. Surf. Sci.*, **375**, 144 (2016).
14. H. Xiao, H. Peng, S. Deng, X. Yang, Y. Zhang and Y. Li, *Bioresour. Technol.*, **111**, 127 (2012).
15. M. M. Yeganeh, T. Kaghazchi and M. Soleimani, *Chem. Eng. Technol.*, **29**, 1247 (2006).
16. J. Cañellas, A. Femenia, C. Rosselló and L. Soler, *J. Sci. Food Agric.*, **59**, 269 (1992).
17. L. Fan, J. Chen, J. Guo, X. Jiang and W. Jiang, *J. Anal. Appl. Pyrol.*, **104**, 353 (2013).
18. G. Nazari, H. Abolghasemi, M. Esmaieli and M. Assar, *Water Treat.*, **57**, 27339 (2016).
19. P. S. Thue, G. S. dos Reis, E. C. Lima, J. M. Sieliechi, G. L. Dotto, A. G. N. Wamba, S. L. P. Dias and F. A. Pavan, *Res. Chem. Intermediat.*, **43**, 1 (2016).
20. M. Asadullah, I. Jahan, M. B. Ahmed, P. Adawiyah, N. H. Malek and M. S. Rahman, *Ind. Eng. Chem. Res.*, **20**, 887 (2014).
21. H. R. Yu, S. Cho, M. J. Jung and Y. S. Lee, *Micropor. Mesopor. Mater.*, **172**, 131 (2013).
22. W. Yang, Y. Wang, P. Sharma, B. Li and K. Liu, *Colloid Surface A.*, **530**, 146 (2017).
23. Q. Liu, T. Zheng, P. Wang and L. Guo, *Ind. Crop. Prod.*, **31**, 233 (2010).
24. X. Wei, Z. Wu, Z. Wu and B. Ye, *Powder Technol.*, **329**, 207 (2018).
25. B. Chen, D. Zhou and L. Zhu, *Environ. Sci. Technol.*, **42**, 5137 (2008).
26. S. E. Elhafez, H. A. Hamad, A. A. Zaatout and G. F. Malash, *Environ. Sci. Pollut. Res. Int.*, **24**, 1 (2017).
27. Y. S. Ho, *J. Hazard. Mater.*, **136**, 681 (2006).
28. A. M. Dowaidar, M. S. EI-Shahawi and I. Ashour, *Sci. Technol.*, **42**,

3609 (2007).
29. P. Ramachandran, R. Vairamuthu and S. Ponnusamy, *J. Eng. Appl. Sci.*, **6**, 15 (2011).
30. I. A. Tan, A. L. Ahmad and B. H. Hameed, *J. Hazard. Mater.*, **164**, 473 (2009).
31. I. A. W. Tan, J. C. Chan, B. H. Hameed and L. L. P. Lim, *J. Water Process Eng.*, **14**, 60 (2016).
32. M. Zhu, J. Yao, L. Dong and J. Sun, *Chemosphere*, **144**, 1645 (2016).
33. M. Ghaedi, A. Daneshyar, A. Asfaram and M. K. Purkait, *Rsc. Adv.*, **6**, 54322 (2016).
34. C. Valderrama, X. Gamisans, X. de las Heras, A. Farrán and J. L. Cortina, *J. Hazard. Mater.*, **157**, 386 (2008).
35. Y. N. Prajapati, B. Bhaduri, H. C. Joshi, A. Srivastava and N. Verma, *Chemosphere*, **155**, 62 (2016).
36. E. K. Radwan, H. Hany, A. Ghafar, A. S. Moursy, C. H. Langford, A. H. Bedair and G. Achari, *Environ. Sci. Pollut. R.*, **22**, 12035 (2015).
37. X. Yang, J. Li, T. Wen, X. Ren, Y. Huang and X. Wang, *Colloids Surf., A.*, **422**, 1 (2013).
38. Y. Zhou, P. Lu and J. Lu, *Carbohyd. Polym.*, **88**, 502 (2012).
39. M. Zhu, W. Tian, H. Chai and J. Yao, *Korean J. Chem. Eng.*, **34**, 1073 (2017).